PNAS
www.pnas.org

Supplementary Information for

Disappearance of the Last Tropical Glaciers in the Western Pacific Warm Pool (Papua, Indonesia) Appears Imminent

Donaldi S. Permana*, Lonnie G. Thompson*, Ellen Mosley-Thompson, Mary E. Davis, Ping-Nan Lin, Julien P. Nicolas, John F. Bolzan, Broxton W. Bird, Vladimir N. Mikhalenko, Paolo Gabrielli, Victor Zagorodnov, Keith R. Mountain, Ulrich Schotterer, Wido Hanggoro, Muhammad N. Habibie, Yohanes Kaize, Dodo Gunawan, Gesang Setyadi, Raden D. Susanto, Alfonso Fernández and Bryan G. Mark

***Corresponding Authors**:
Donaldi S. Permana
Center for Research and Development
Agency for Meteorology Climatology and Geophysics (BMKG)
Jl. Angkasa I No.2 Kemayoran, Jakarta 10720
Phone : (+62) 856 911 72931
E-mail addresses: donaldi.permana@bmkg.go.id, permana.5@osu.edu

Lonnie G. Thompson
Byrd Polar and Climate Research Center (BPCRC)
The Ohio State University
1090 Carmack Rd, Columbus, OH 43210, USA
Phone : (+1) 614 292 6652
E-mail address: thompson.3@osu.edu

This PDF file includes:

- Supplementary text
- Figs. S1 to S12
- Table S1 to S6

www.pnas.org/cgi/doi/10.1073/pnas.1822037116

Supplementary Text

Determination of changes in ice surface area

Background image (Fig. 3*A*) was derived from http://eoimages.gsfc.nasa.gov/images/imagerecords/79000/79084/grasberg_tm5_2009301_lrg.jpg. Details of five satellite images used to outline and quantify the surface area of the Puncak Jaya glaciers (Fig. 3*B* and *C*) are in Table S1. The 2002 image was extracted from Google Maps as a flat image (stereoscopic 3D mode turned off). All images were obtained as orthorectified products. To correct for residual relief displacement not removed through orthorectification, IKONOS and WorldView-2/3 images were manually co-registered with respect to Planet's May 2016 image using clearly identifiable topographic features (a similar approach for the same area was used in (1)). For area calculations, the five images were mapped in a Universal Transverse Mercator (UTM) projection (zone 53 S) using the World Geodetic System 1984 (WGS84) datum. All image processing and area calculations were performed using the QGIS software (version 3).

Simulation of glacier volumetric changes

Volumetric changes from 2017 to 2030 were simulated with a spatially distributed model that calculates mass balance (in meters water equivalent or m.w.e.) at daily time steps on each grid-cell flagged as ice or snow, according to the Randolph Glacier Inventory (RGI) (2). Ablation (*Ab*) is computed from daily positive temperatures while accumulation (*Ac*) utilizes temperature thresholds to determine the amount of solid precipitation falling over the glacierized area:

$$Ab = \text{DDF} \times T_a \ if\ T_a \geq 0°C \qquad \text{Eq. 1}$$

$$Ab = 0 \ if\ T_a < 0°C \qquad \text{Eq. 2}$$

$$Ac = Pp \ \ if\ \ T_a < T_{sf} \qquad \text{Eq. 3}$$

$$Ac = Pp\left(\frac{T_r - T_a}{T_r - T_{sf}}\right) \ if\ T_{sf} < T_a < T_r \qquad \text{Eq. 4}$$

$$Ac = 0 \ if\ T_a \geq T_r \qquad \text{Eq. 5}$$

DDF is the Degree Day Factor (m d^{-1} $°C^{-1}$), which converts air temperature into ablation; T_{sf}, is the temperature threshold for accumulation while and T_r is the threshold for rain. T_{sf} and T_r were assumed to be 0°C and 2°C. Computation of daily melt utilized different DDFs: (a) snow on grid-cells that had accumulation the previous day and otherwise (b) for ice.

Modeled elevation changes were converted into volume (in km^3) and transformed into a ratio relative to an initial ice volume computed from a volume-area scaling (3-4) and estimated as 0.13 km^3. This class of semi-empirical model was selected following recommendations (5) regarding quality and quantity of available data and the length of calibration periods for model evaluation. Here, the climatic data available and the relatively flat topography allowed us to infer that (a) most, if not all, ablation occurs as melt, and (b) relatively short windows for calibration and validation are available from 1997 to 2016.

The ASTERGDEM (6) (30-meter grid-cell size) provided the regional topographic representation. Time series for precipitation and temperature were derived from available observations and downscaled global climate model simulations (see below).

Mass balance model calibration

The model was calibrated by simulating periods with available stake measurements and we sought optimal combinations of lapse rates and DDFs that reproduced the surface thinning. One thousand combinations were tested using lapse rates provided by Fig. S3 and published DDFs (7). The model reproduced observed thinning with a relatively small bias. Optimal parameters were identified using a quasi-zero temperature lapse rate and precipitation lapse rate similar to the mean detected between DISP and ALP (Fig. S3). Average DDF for snow (ice) was fairly consistent (more variable) among the simulated periods. Only the May 2016 – November 2016 simulation showed a logical pattern of higher DDF for snow versus ice, thus the simulated parameters for this period were employed in future change simulations (Table S3). This optimal combination of parameters suggested that temperatures do not change significantly over the ice fields, in sharp contrast with the average lapse rates for the pair DISP-ALP (Fig. S3). To test the sensitivity of the results to other realistic lapse rates, two additional temperature lapse rates were utilized: 4.6°C/km, corresponding to the mean between GRS-DISP and GRS-ALP, and the environmental lapse rate (6.5°C/km).

The climatic records for mass balance model input

Precipitation and temperature records around the study area are short and discontinuous (Table S2) and were combined to construct a relatively continuous time series for the highest elevation weather station (ALP). Daily lapse rates were computed between each pair of stations to examine the relationship with elevation. Lapse rates for precipitation vary considerably, with some extreme values well above ±150 mm/km while for temperature they are more concentrated around the mean (close to the environmental lapse rate for the pair DISP-ALP, Fig. S3). ALP reconstruction used a multilinear regression with GRS and DISP as predictors. Linear regressions of the daily values between each pair of records explain 45% to 66% of the variance for precipitation and 50% to 66% of the variance for temperature (Fig. S6). The reconstructed ALP record (henceforth, rALP) covers 88% of the period 1999-2016 for both variables, a significantly longer time series than the original ALP record (< 75% for precipitation and < than 60% for temperature), therefore maximizing the number of calibration periods utilized for the modeling. From the remaining gaps (12% for 1999-2016), 0.5% and 0.7% are isolated records of precipitation and temperature, respectively; these records were filled by linear interpolation using values from the previous and subsequent days. Fig. S7 shows that ALP and rALP time series are significantly correlated and the Nash–Sutcliffe model efficiency coefficient is close to 1 for both variables. Simulation of future volume change was performed for the period 2017-2030 using input from climate model projections, described in the next section.

Downscaling of global climate projections for the region

Southeast Asia Regional Climate Downscaling (SEACLID) / Coordinated Regional Climate Downscaling Experiment-Southeast Asia (CORDEX-SEA) project (8-11) (http://www.ukm.edu.my/seaclid-cordex, http://www.apn-gcr.org/resources/items/show/1886) provides output from regional atmospheric model simulations over Southeast Asia that were forced by output from global climate model experiments conducted by the Coupled Model Intercomparison Project Phase 5 [CMIP5 (12)]. The horizontal grid spacing of the regional model output is 25 km. The data were downloaded from the Earth System Grid node of Linköping University (https://esg-dn1.nsc.liu.se/search/esgf-liu/) and derived from CORDEX-SEA dataset (as in (11)). Daily estimates of precipitation and 2-meter temperature from five models and for three CMIP5 experiments (historical, RCP4.5, and RCP8.5) (Table S4) were used. Time series for the Puncak Jaya ice fields were obtained from bilinear interpolation of the gridded model output, and then downscaled using the cumulative distribution function (CDF)-Transform (CDFt) method (13). The 1999-2005 period was used for calibration while the 2006-2016 period was used for validation. The bounds of the calibration period were dictated by the beginning of the rALP record (1999) and the end of the CMIP5/CORDEX historical runs (2005). Validation included comparison between the 2006-2016 downscaled time series (RCP4.5 and RCP8.5) with rALP. Following (13), the skill of the models was assessed using the Cramér-von Mises test with α=0.05, in which a p-value greater than this significance level means that downscaled and observed time series are not statistically different. The CSIROMK36-REGCM4 model exhibits the best overall skill for both RCP scenarios (highest *p*-values). All other downscaled time series were less consistent with observations (see Table S4 for details). The model predicts that under practically all scenarios glacier shrinkage will continue unabated, leading to total ice loss no later than 2026 (Fig. S8). It is important to remember that the model had been tuned during a period of accelerated thinning (Table S3) based on the available meteorological data (GRS, DISP and ALP stations) in the highland, which in itself infers a somewhat anomalously high amount of energy on the ice surface. As a tunable value given the scarcity of data, the rate of 0.1°C/km indicates that the melting conditions were more or less similar across the study area. After considering the data for the model, the elevation of 4366 m was used for the pole site, which is just within 4 meters of the nominal elevation of the ALP station (~4400 m). That also supports the low lapse rate, because the elevation is practically the same. Even with a more accurate ALP elevation, the result (~+/-30 m) would not be significantly different. The hypsometric distributions demonstrate that the elevation range of the glacierized region is ~400 m (except ASTERGDEM, where less than 10% of the area is above that range, Fig S4). Therefore, it is essentially flat and thus justifies a low lapse rate as well.

Figure S8 shows somewhat erratic performances of IPSL and especially MPI. Different runs of RegCM4 performed by CORDEX-SEA members were statistically downscaled and forced, in turn, by different model output from GCMs (see Table S4). After performing the statistical downscaling, the bias of both combinations, IPSL-

RegCM4 and MPI-RegCM4, relative to observations, was observed during the validation period (2006-2016). IPSL-RegCM4 shows a negative bias (colder than observations) in the RCP8.5 while there is a positive bias in RCP4.5 (warmer than observations). This would explain less melting in the RCP8.5 scenario. For MPI-RegCM4, the bias is noticeable in precipitation, with RCP8.5 being almost 5 five times larger than RCP4.5, and thus during the simulation any temperature below freezing implies much more accumulation in RCP8.5. All other models have consistent biases in both scenarios and thus provide a more coherent behavior of glacier mass balance. One of the co-authors (Alfonso Fernández) has been working over the last year with data from the RegCM4 model (the same model utilized by CORDEX-SEA members to dynamically downscale the global models to the versions used in the paper) for downscaling MPI for Chile (i.e., the same combination MPI-RegCM4 from Table S4). Inconsistency in precipitation was found which is similar to the Puncak Jaya case where the RCP8.5 (more pessimistic scenario) produces more precipitation than RCP4.5. In Puncak Jaya case, RCP8.5 shows a larger positive bias (2.72 mm/day) relative to RCP4.5 (0.6 mm/day). In both cases (Puncak Jaya and Chile), this is counterintuitive as drier conditions should be expected in the RCP8.5 as most models predict, despite large interannual variability. This problem is so important to consider that the institute producing the MPI-RegCM4 simulations for Chile had to add a disclaimer message on their website (http://simulaciones.cr2.cl/). These two coincidental results with the combination MPI-RegCM4 suggest that one of the models (MPI or RegCM4) might be generating some biases.

Ice core sample analysis

Ice cores were cut into discrete samples, melted, and analyzed for oxygen and hydrogen isotope ratios ($\delta^{18}O$, δD, respectively), and insoluble dust and major anion and cation concentrations. All measurements were conducted in BPCRC laboratories. $\delta^{18}O$ and δD were measured using a Thermo Finnigan mass spectrometer and a Picarro cavity ring-down spectroscopy analyzer. Analyses of identical samples using both machines agreed well (14). The concentrations of insoluble dust particles from 0.63 to 20 µm in diameter were measured using a Beckman-Coulter Multisizer 4. The concentrations of the major cations (NH_4^+, Na^+, K^+, Mg^{2+}, and Ca^{2+}) and anions (SO_4^{2-}, NO_3^-, F^-, and Cl^-) were determined using a Dionex ICS-3000 ion chromatograph. Descriptions of the sample handling procedures and data collection are in (14).

Core D1 was cut into three sets of 1156 co-registered samples (each ~2.8 cm long) which were analyzed for stable isotopes, insoluble dust, and major ions. Tritium (^3H) concentrations for 68 samples (Core D1) were measured at the Division of Climate and Environmental Physics, Physics Institute, University of Bern, Switzerland to locate the 1960s thermonuclear bomb test horizons. Core D1B contains 1607 co-registered samples (each ~2 cm long) which were analyzed for stable isotopes and dust. Major ions were analyzed for 644 samples (each ~5 cm long).

Reproducibility of $\delta^{18}O$, δD, and dust concentrations between Cores D1 and D1B

The $\delta^{18}O$ and δD profiles of Cores D1 and D1B show similar variations, with moderate stable isotopic variability (5 to 6‰ and 45 to 50‰, respectively) (Fig. 4*A* and *B*). Their $\delta^{18}O$ averages (-16.07 to -16.41‰, respectively; Table S5) are similar to the 1-

meter $\delta^{18}O$ averages from the 1972 Meren and Cartensz Glacier cores (-15.7‰) (15) before surface melting was a major issue and arguing that the climatic records are likely well preserved in both cores. Large isotopic depletions occur at depths of 8, 12, 17 and 26 meters. Stable isotopic ratios in both cores show gradual but significant enrichment in the top eight meters and significant smoothing in the top four meters. Both cores are composed entirely of ice, with no observable firn and no vertically elongated, or otherwise deformed, bubbles. The high-resolution insoluble dust record from Core D1 illustrates prominent events from 20 to 29 m depth and in the top eight meters (Fig. 4*C*), as do the records of major ion concentrations (14). The considerable isotopic smoothing in the upper part of the cores and very low aerosol concentrations below 4 meters suggest that substantial post-depositional alteration has occurred in this upper section.

Post-depositional processes (e.g., evaporation, melting, and rainfall) may alter the climate record in an ice core (16). However, these records indicate that the impact of these processes is limited below ~4 m depth, and suggest that the climatic and environmental records are at least partially preserved. This is similar to the climate record from the Furtwängler Glacier on Kilimanjaro. During the drilling of the Furtwängler Glacier water was encountered throughout the borehole and most soluble ions in the ice column were removed, most likely by post-depositional melting (17). However, the climate record from $\delta^{18}O$ had remained intact if rather muted compared with the records from the larger ice fields on Kilimanjaro. Additional support for the viability of the record in the ENF cores comes from the lack of sharp bomb peaks in the pre-1964 tritium measurements in Core D1 (Fig. 5*A*) which argues against post-depositional melting and refreezing at lower depths (18). Core D1 is the cleanest tropical ice core yet recovered by BPCRC, even more so than the Quelccaya (19) and the Kilimanjaro cores (17). This likely reflects the surrounding oceans which provide few sources of dust and soluble aerosols (14), very heavy annual rainfall, and possible elution of ions and dust due to post-depositional processes.

<u>Timescale reconstruction – tritium (^3H) analysis</u>

In the mid-1950s and early 1960s, ^3H was widely dispersed during above-ground atomic bomb testing. The quantity of ^3H in the atmosphere peaked in 1962 – 1963 and has decreased thereafter. The 1962/63 peak is routinely used as a global chronological marker for dating ice cores. In New Guinea Island, there were two GNIP IAEA/WMO stations which recorded ^3H: Jayapura (2.53°S; 140.72°E; 3 m.a.s.l), ~435 km northeast of the drill sites (1957 – 1991) and Madang (5.22°S; 145.80°E; 4 m.a.s.l), ~950 km east of the drill sites (1968 – 1982) (Fig. S9*A*). Jayapura station recorded high ^3H concentrations (~33 TU) in precipitation in 1964 (Fig. S9*B*) suggesting the glaciers near Puncak Jaya likely preserve this signal. Sixty-eight Core D1 samples (each ~0.47 m long) were analyzed for ^3H concentrations and reveal a peak (2.98 ± 0.42 TU) recorded at 23.4 m (Fig. 5*A*). Since tritium has a half-life of 12.3 years, after 47 years (from 1964 to 2010) the tritium concentration in precipitation in 1964 would become (33 TU) ^ (1/ (47/12.3)) ≈ 2.49 TU which is comparable with the tritium peak recorded in Core D1 at a depth of 23.4 m (Fig. S9*C*). The differences in background concentrations below 26 m and above 22 m strongly suggest that the bomb tests elevated the natural ^3H background level thus providing an absolute time marker of 1964 at 23.4 m in Core D1.

Timescale reconstruction – $\delta^{18}O$ reference matching with NINO3 ERSST

The annual means of $\delta^{18}O$ of precipitation (thermal year which covers the period of August of previous year to July of the current year) from the GNIP station at Jayapura (1961-1991) were compared with NINO3 ERSST (http://www.esrl.noaa.gov/psd/data/gridded/data.noaa.ersst.v4.html) (Fig. S10). The precipitation $\delta^{18}O$ at Jayapura is only available from 1961 to 1991. Peak $\delta^{18}O$ enrichments recorded in precipitation from 1972-1973 and 1982-1984 at Jayapura are likely associated with strong El Niño events in 1972-73 and 1982-83, respectively (14). The correlation field between the annual rainfall $\delta^{18}O$ at Jayapura and ERSST from 1961 to 1991 (31 years) is shown in Fig. S10*A*. By implementing the non-parametric approach for data that are serially correlated (20), the annual rainfall $\delta^{18}O$ at Jayapura has relatively significant positive correlation with NINO3 ERSST (Area A in Fig S10*A*) ($R = 0.31$; $p = 0.09$) and average SSTs over the region of 5-20°S and 120-90°W (Area B in Fig S10*A*) ($R = 0.36$; $p = 0.05$) in the eastern Pacific. The annual rainfall $\delta^{18}O$ at Jayapura is also negatively correlated with average SSTs in southeast New Guinea (Area C in Fig S10*A*, 6-18°S; 140-160°E). This indicates that there is a link between rainfall $\delta^{18}O$ at Jayapura and the ENSO indices, with increased rainfall $\delta^{18}O$ during El Niño conditions, and more depleted $\delta^{18}O$ during normal and La Niña conditions. This relationship was supported by previous studies in Papua (21) and lowland Borneo (22). Thus, for simplicity, the NINO3 ERSST time series was used as a matching reference to construct the timescale for the Papua ice cores. The $\delta^{18}O$ data at fourteen points in Core D1 were paired with the 13-month running means of NINO3 ERSST by assigning the ^{3}H peak at 23.4 meters depth as the 1964 bomb horizon (Fig. 5*A*), and assuming the top layer represents the time when the ice cores were collected (May 2010) (Fig. 5*B*). Along with these two points, the twelve points consisted of seven El Niño events (2002/2003, 1997/1998, 1991/1992, 1987/1988, 1982/1983, 1972/1973 and 1965/1966) and five La Niña events (2007/2008, 1999/2000, 1995/1996, 1988/1989 and 1975/1976) (Table S6). Each time series was developed using linear interpolation between matching points. Annually resolved stable isotope, dust, and major ion records since 1964 were calculated by averaging values within each year. The depth-age relationships for the Papua ice cores are shown in Fig. S11. The timescale was independently checked by comparing the Core D1 tritium record with tritium from precipitation collected at GNIP stations in Jayapura in Indonesia and Madang in Papua New Guinea (Fig. 6).

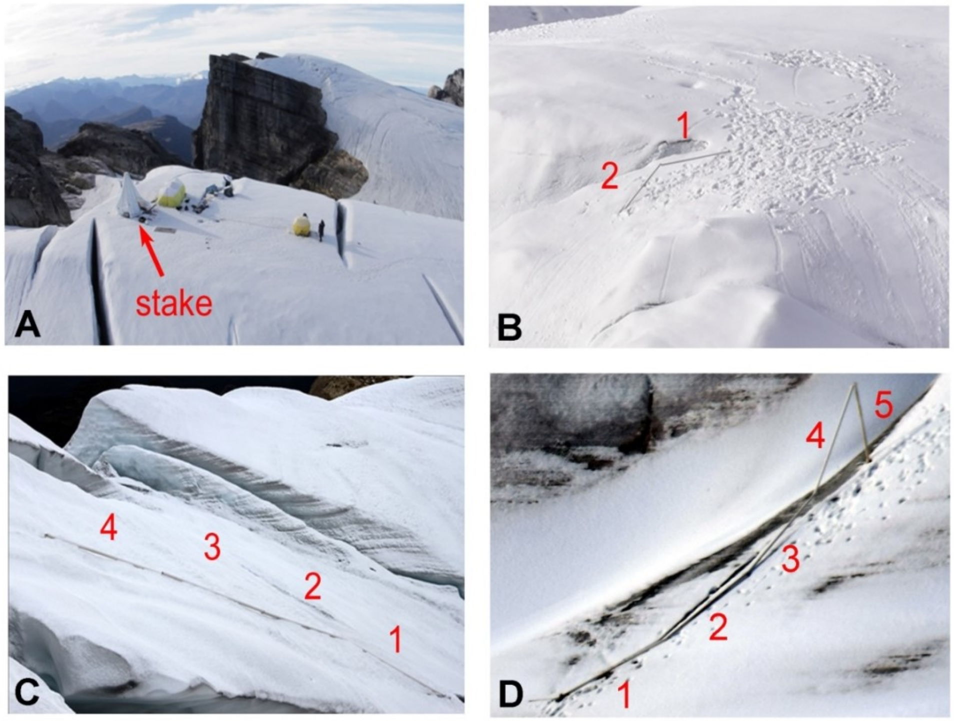

Figure S1 | Thinning of the East Northwall Firn from 2010 to 2016. The increasing exposure of the upper sections of an articulated PVC stake placed in a borehole in June 2010 (A) is shown in November 2015 (B), in May 2016 (C), and in November 2016 (D). The exposed two-meter PVC sections shown in (B), (C) and (D) are numbered. Note that the photographs of the stake were taken from different angles by Dave Christensen and Greg Chimura (A), Yohanes Kaize (B, C) and Donaldi Permana (D).

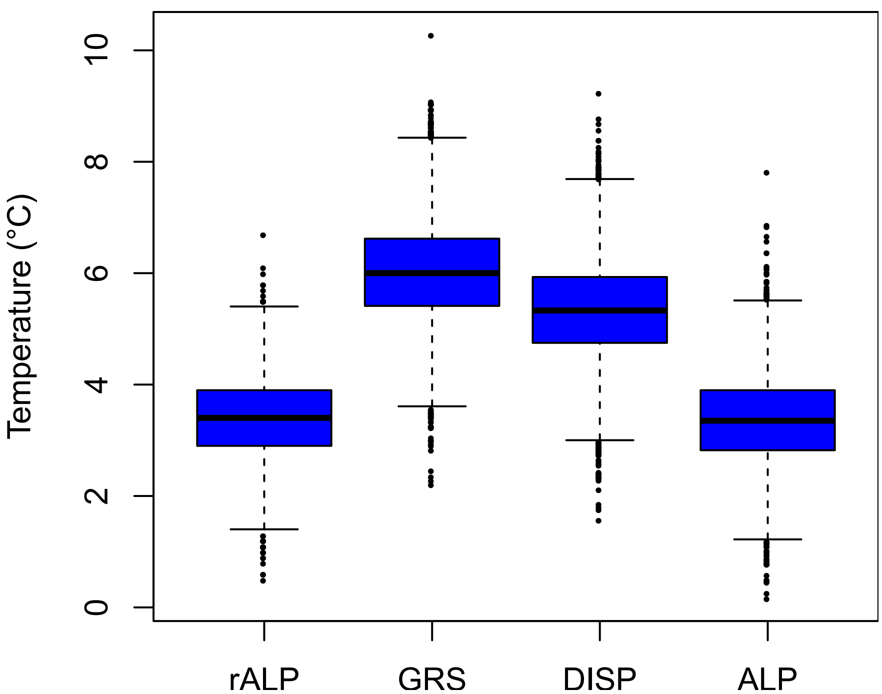

Figure S2 | Distribution of available temperature records from 1997 to 2016 (rALP - reconstructed ALP is included for reference; see Supplementary Text, Table S2 and Figs. S6 to S7). They show no daily-averaged temperatures below freezing through this period. A bootstrapped Kolmogorov-Smirnov test (1000 iterations sampling 90% of the data) applied to each time series indicates that they can be modeled by a normal distribution with a significance level of 0.01. The probabilities (%) of below freezing temperatures calculated from the corresponding normal distribution are 3.7×10^{-9} for GRS, 2.6×10^{-7} for DISP, and 0.005 for ALP.

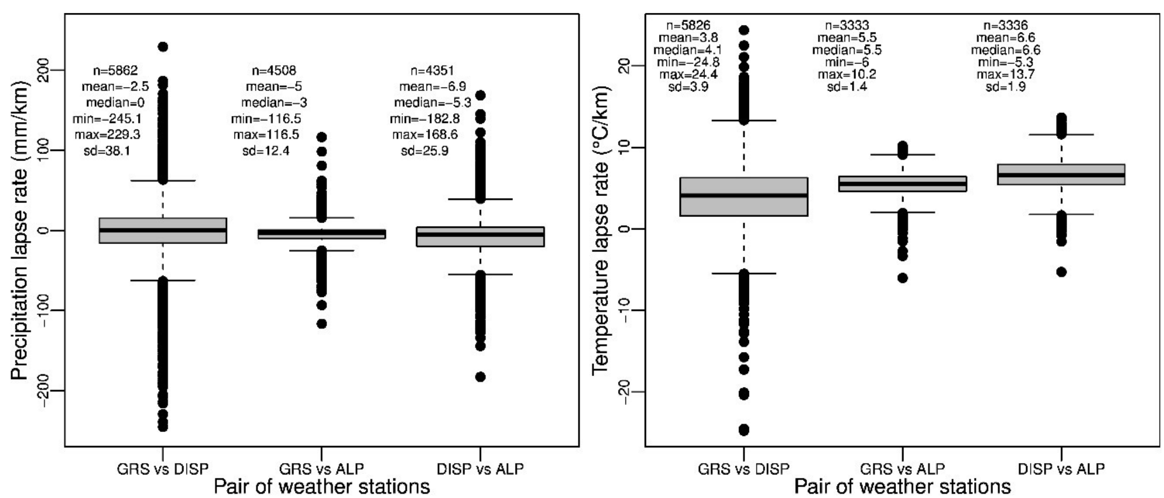

Figure S3 | Distribution of daily lapse rates for precipitation and temperature for each pair of stations located in the study area. Positive values indicate a decrease in the variable according to elevation while negative values indicate an increase.

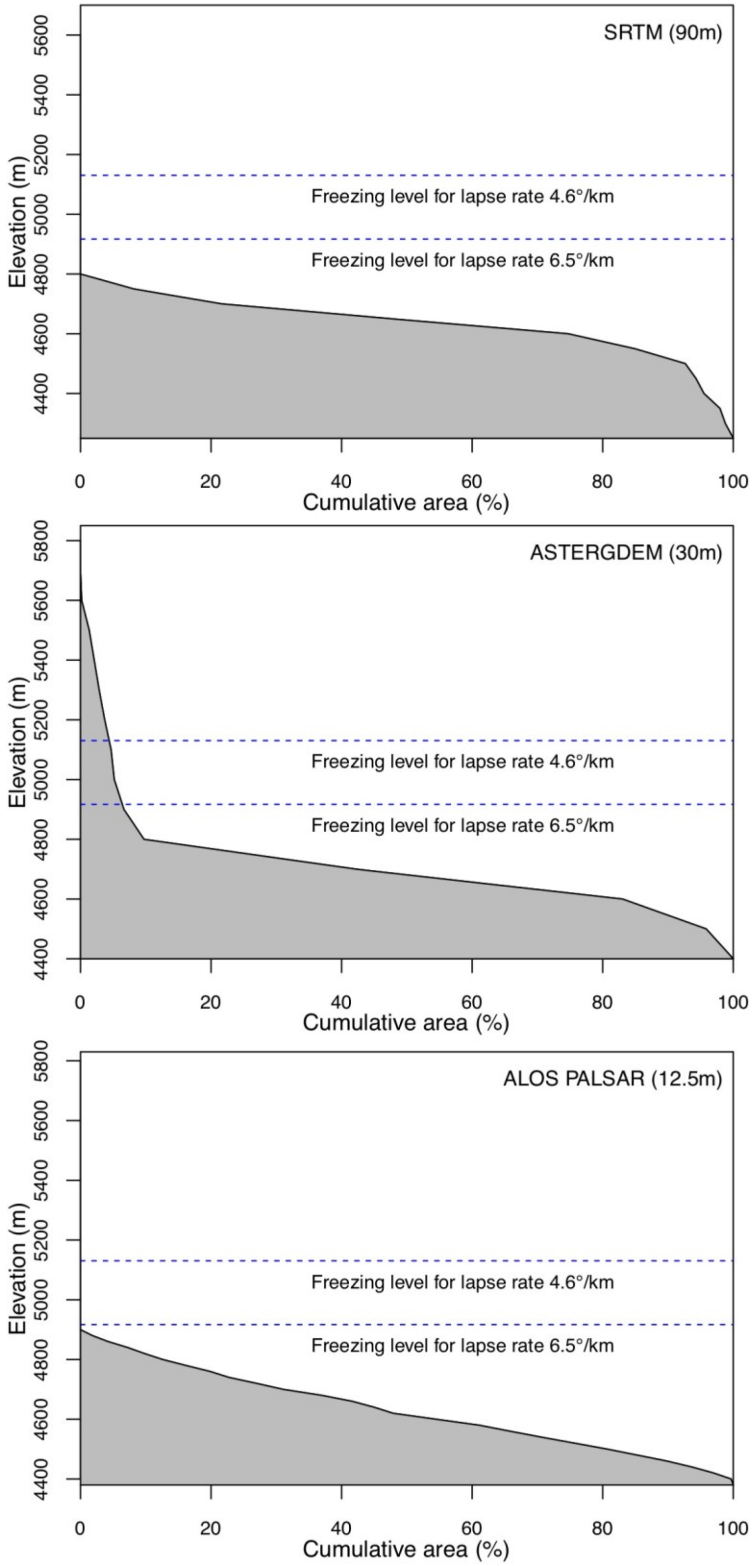
SRTM (90m)
Freezing level for lapse rate 4.6°/km
Freezing level for lapse rate 6.5°/km
Elevation (m)
Cumulative area (%)
ASTERGDEM (30m)
Freezing level for lapse rate 4.6°/km
Freezing level for lapse rate 6.5°/km
Elevation (m)
Cumulative area (%)
ALOS PALSAR (12.5m)
Freezing level for lapse rate 4.6°/km
Freezing level for lapse rate 6.5°/km
Elevation (m)
Cumulative area (%)

Figure S4 | Hypsometric distribution of the ice covered area in Puncak Jaya according to the available topographic data for the region. Each curve presents the freezing line (dashed blue) as calculated from the average temperature at the ALP station (3.36°C) and using two lapse rates. Hypsometry from ASTERGDEM (6) is the only source of data showing that more than 90% of the remaining glacier surface is below these freezing lines. Hypsometry derived from SRTM (23) and ALOS PALSAR (24) suggests that the remaining glacierized area is persistently affected by melting temperatures.

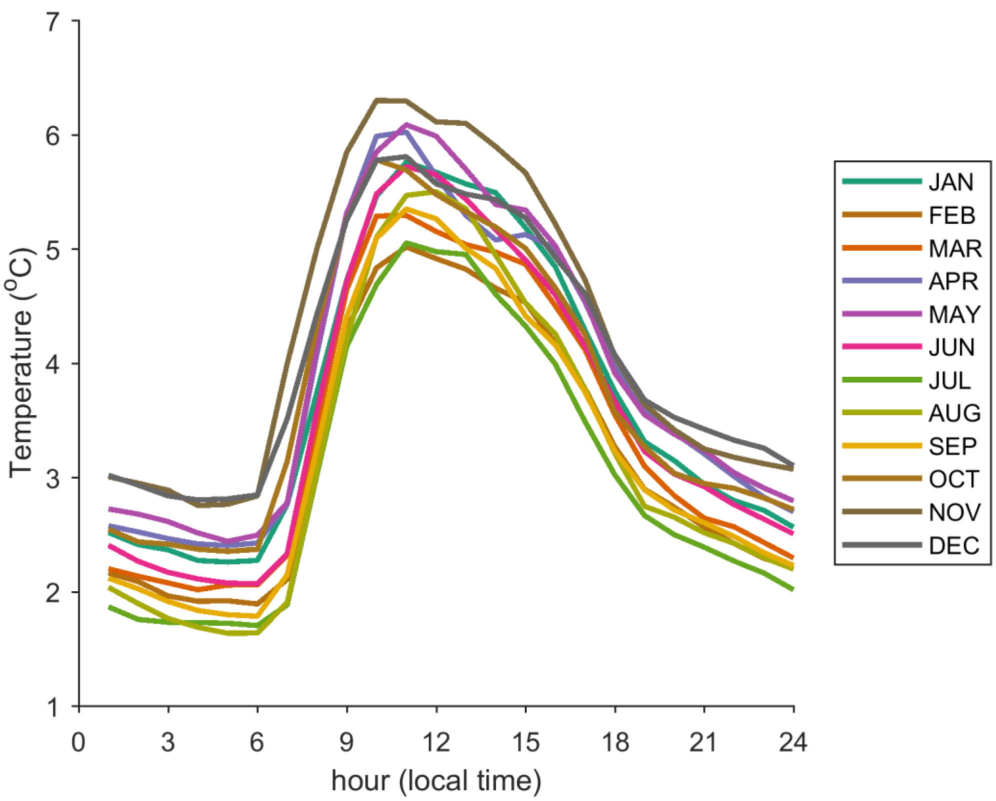

Figure S5 | Diurnal temperature cycle at the ALP station (4,400 masl). Applying different lapse rates (4.6 and 6.5°C/km) to this cycle suggests that melting temperatures occur on most of the glacierized area while below-freezing conditions may predominate at elevations above 4,800 m for 4 to 6 hours in the early morning, particularly from July to September**.**

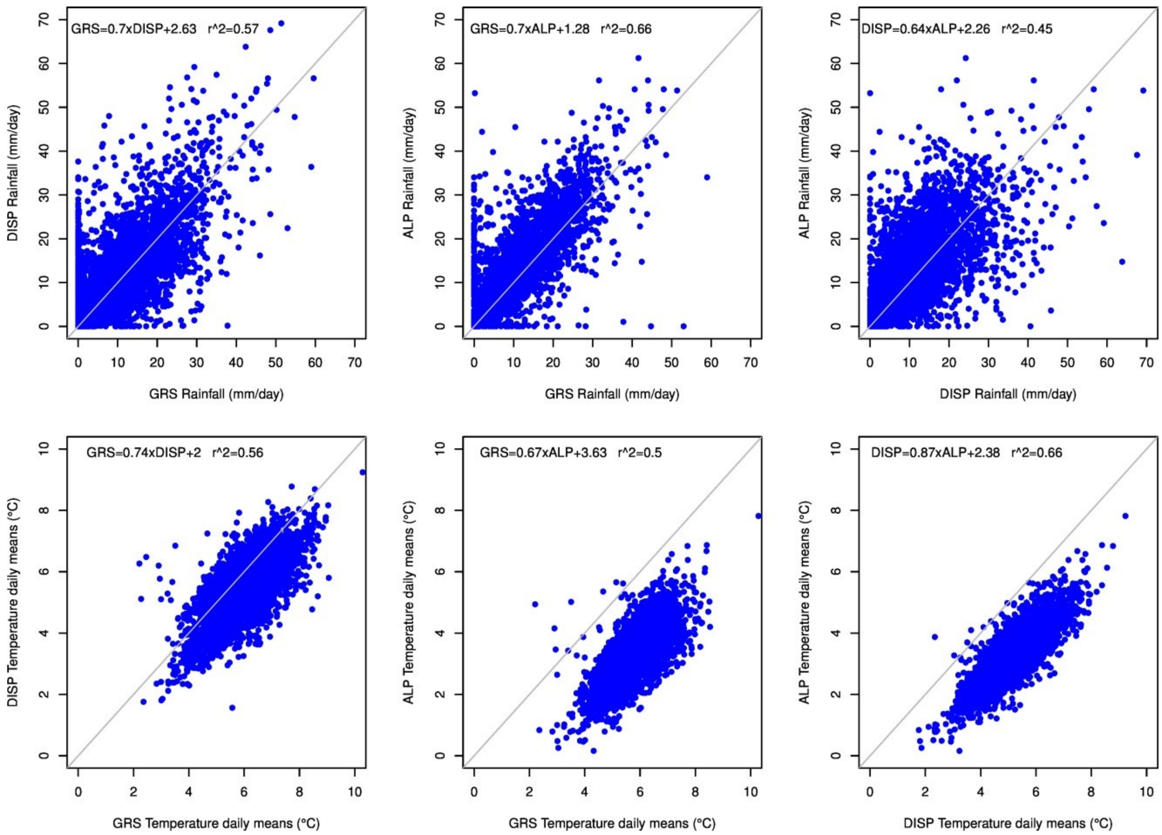

Figure S6 | Linear regression models between each pair of stations at daily resolution. Top panels correspond to models for precipitation while bottom panels correspond to models for temperature.

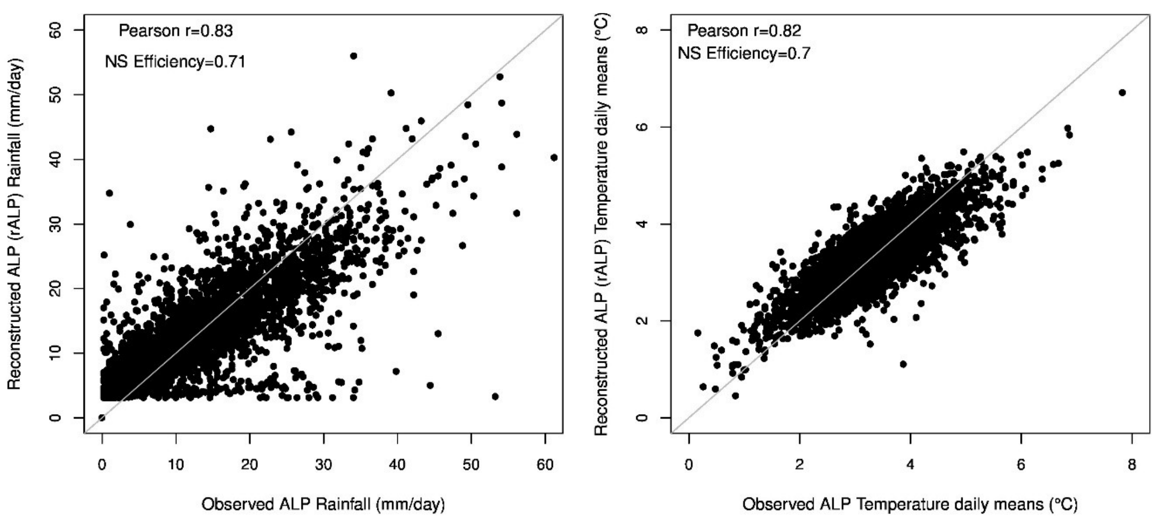

Figure S7 | Comparison between observed (ALP) and modeled (rALP) variables.

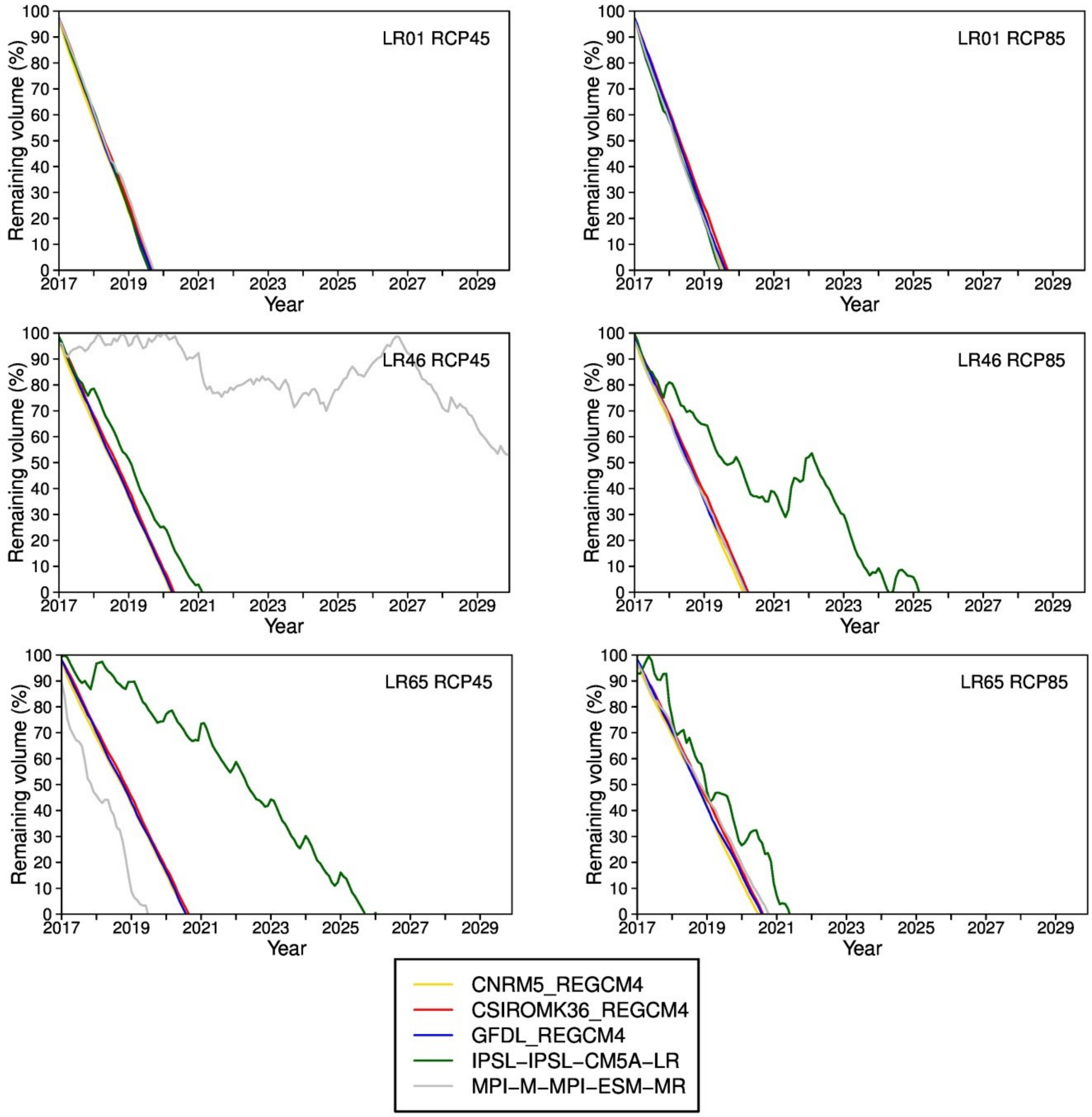

Figure S8 | Results of the mass balance simulations using all combinations of the lapse rates, RCPs, and model projections (see Supplementary Text, Tables S3 and S4). The code of each panel indicates the lapse rate (e.g., LR01 is for a lapse rate of 0.1°C/km) and the RCP scenario utilized in the respective simulation (e.g., RCP45 is RCP4.5). Results predict that across all scenarios glaciers in Puncak Jaya will disappear by 2026 with one exception. The exception is the MPI-M-MPI-ESM-MR, which predicts that 60% of the ice volume will remain after 2030. Model descriptions can be found in (11).

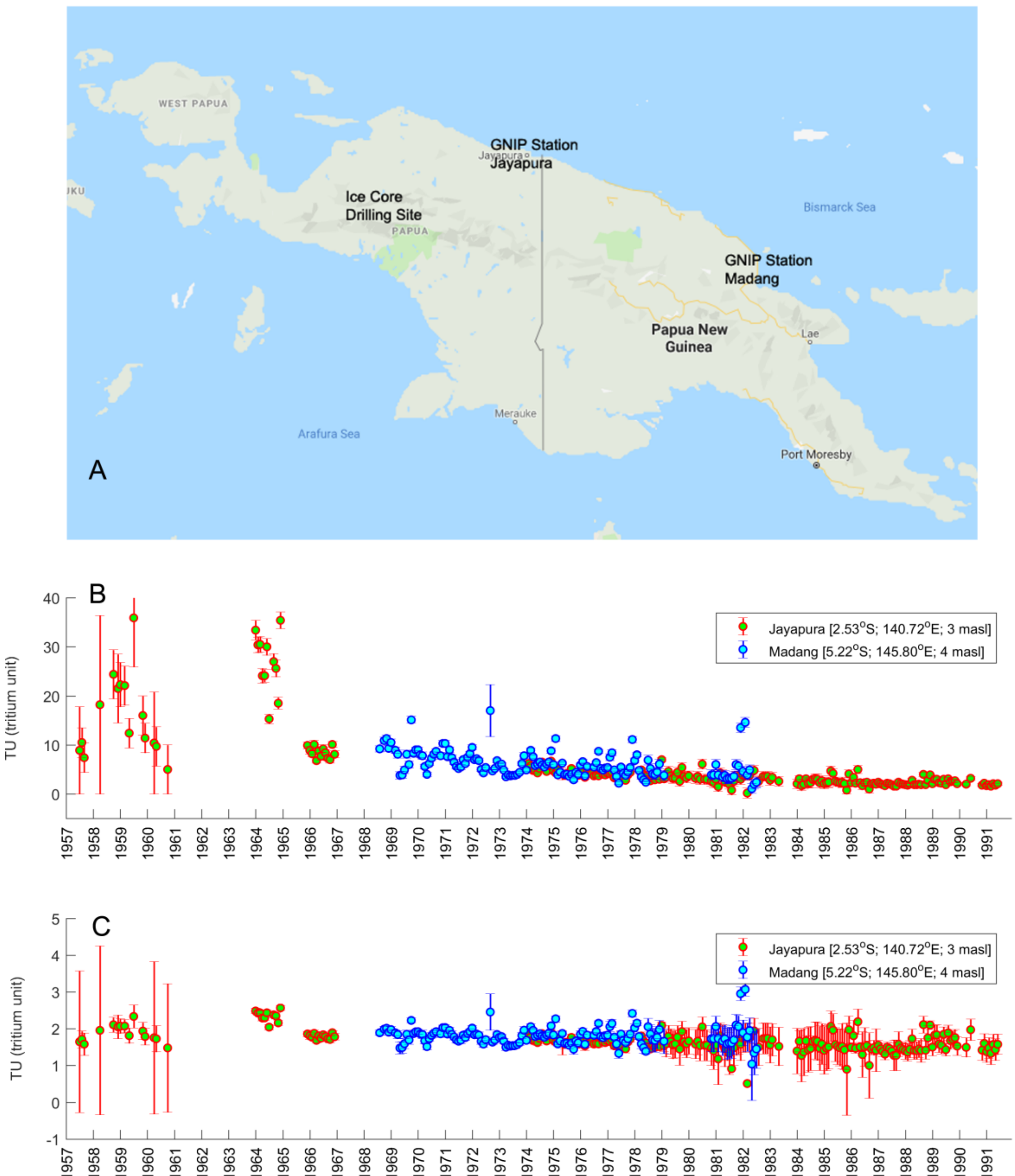

Figure S9 | Tritium concentrations in precipitation at GNIP stations in New Guinea Island. (A) The map of GNIP IAEA/WMO stations at Jayapura, Indonesia and Madang, Papua New Guinea. (B) The monthly tritium concentration in precipitation was recorded at Jayapura and Madang stations from 1957 to 1991. The tritium peak (~33 TU) was recorded in 1964 at Jayapura station. Note that the tritium in precipitation at Madang on September 1968 was removed due to an outliar. (C) As in (B), but reflects the decay of tritium (half-life of 12.3 years) in June 2010 when the ice cores were recovered.

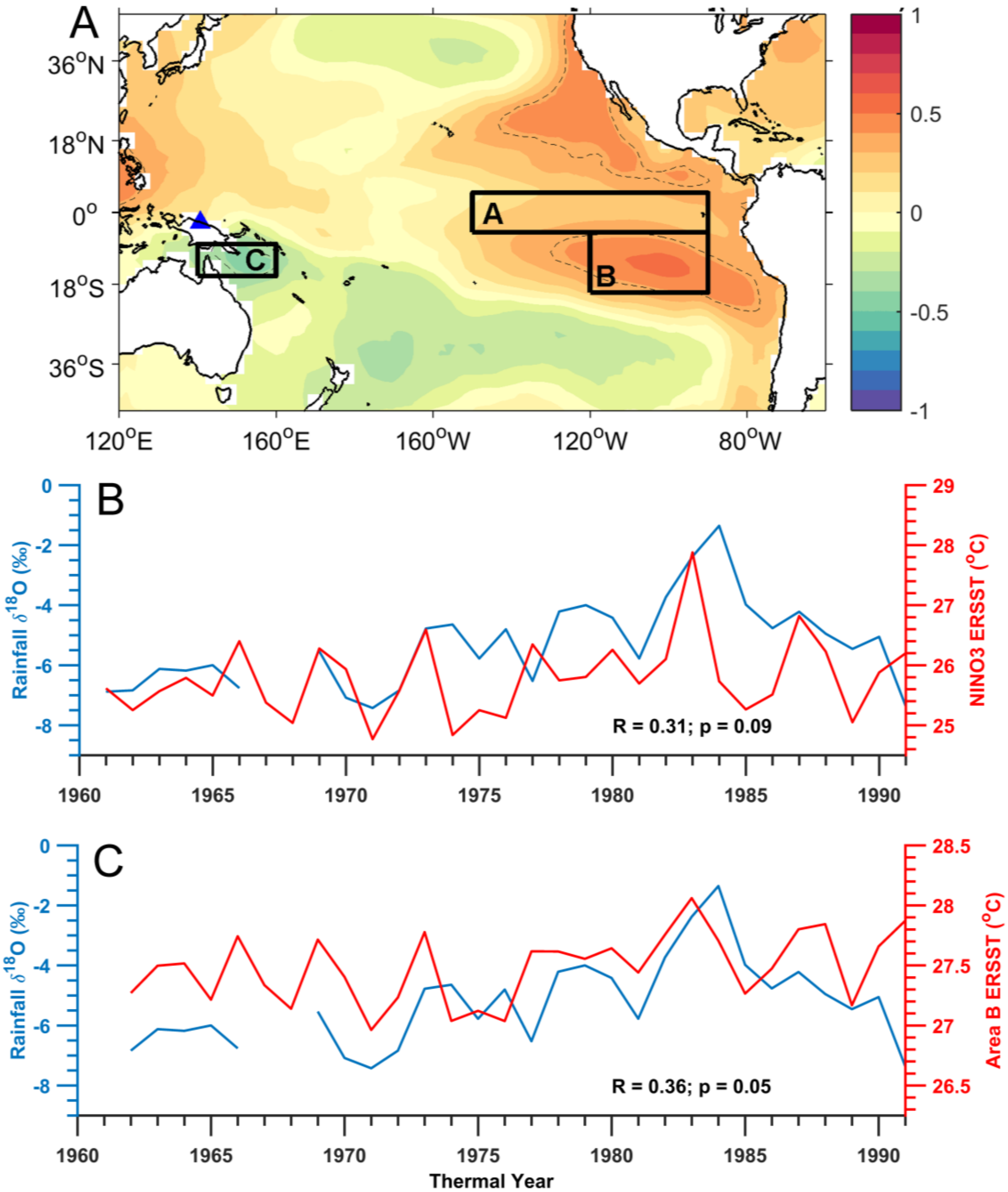

Figure S10 | Comparisons between NINO3 ERSST and rainfall δ^{18}O. (A) The correlation field between annual ERSSTv4 and rainfall δ^{18}O at the GNIP station in Jayapura (2.53°S; 140.72°E; 3 m.a.s.l, blue triangle) from 1961 to 1991 (dashed lines indicate the area with p-values < 0.05). (B) The time series correlation between the rainfall δ^{18}O in Jayapura and the annual NINO3 ERSST (Area A). (C) As in (B), but with the annual mean ERSST of Area B (5-20°S; 120-90°W). Area C (6-18°S; 140-160°E) in Panel (A) indicates a significant negative correlation between rainfall δ^{18}O and ERSST. The thermal year covers the period of August of the previous year to July of the current year.

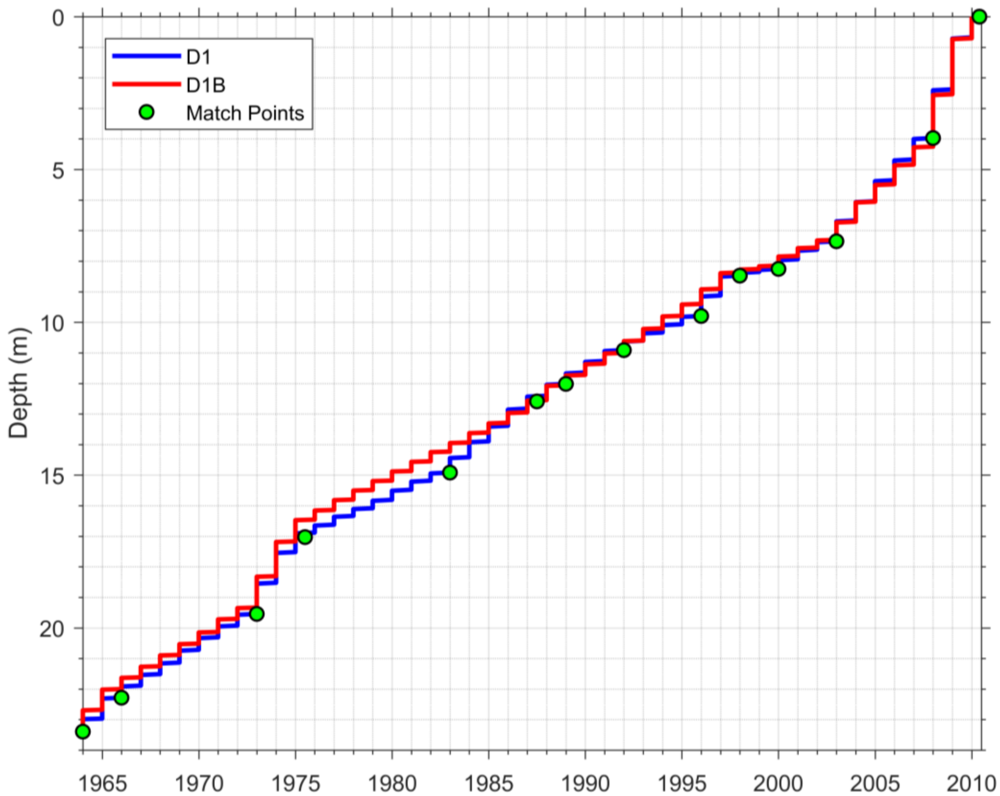

Figure S11 | The depth-age relationships for Cores D1 and D1B. Plots are based on the reference matching timescale in Table S6.

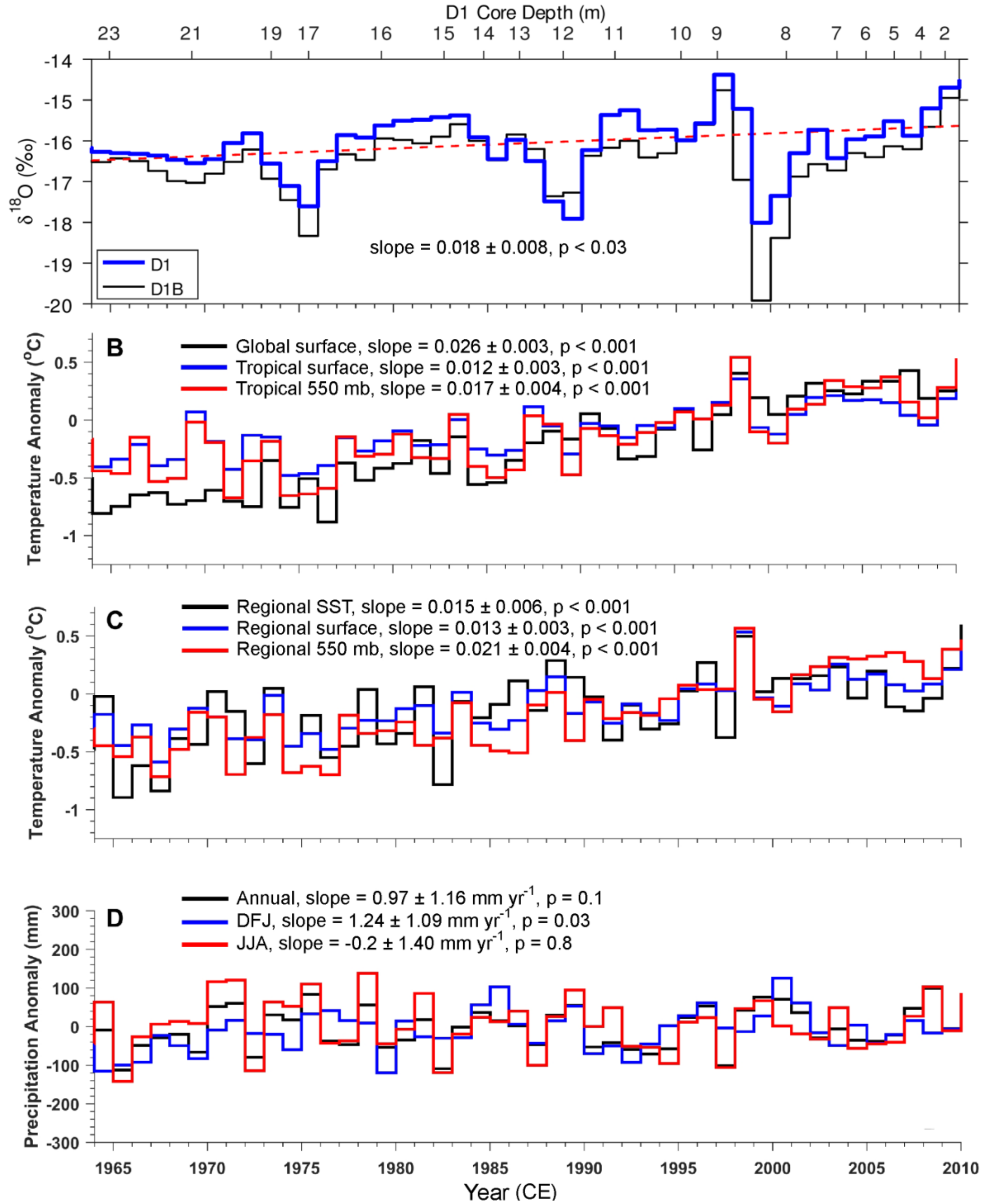

Figure | S12 Comparison of the annual ice core δ^{18}O and temperature records. (A) Annual δ^{18}O of D1 and D1B with the linear trend of D1 (dashed red line). (B) Annual mean temperature anomalies of the global surface (25), the tropical (30°S - 30°N) surface, and the tropical 550-mb level (25). (C) As in (B) but for the sea surface (25), the surface, and the 550-mb level over the Papua glacier region (136 - 138°E; 4 - 6°S). (D) The annual and seasonal mean precipitation anomalies over the Papua glacier region (26).

Table S1 | Characteristics of the satellite images used to determine the surface area of the Papua glaciers

Date	Satellite	Source/Provider	Ground resolution	Off-nadir Angle
11 June 2002	IKONOS	Google Earth	0.8 m	6.6°
16 March 2015	WorldView-3	MapMart.com	0.3 m	15.0°
16 May 2016	Planetscope Doves	Planet.com	2.6 m	1.3°
12 August 2016	WorldView-2	MapMart.com	0.5 m	15.0°
28 March 2018	Planetscope Doves	Planet.com	3.6 m	0.3°

Table S2 | Characteristics of the available climatic records for the study area

		Weather station		
		Grasberg-Nursery (GRS)	Dispatch Tower (DISP)	Alpine (ALP)
	Latitude	4.041 °S	4.068 °S	4.045 °S
	Longitude	137.120 °E	137.114 °E	137.138 °E
	Elevation (m)	3945	4109	4400
Temperature	First date with data	1/1/97	1/1/99	1/1/00
	Last date with data	11/25/16	11/25/16	12/31/16
	Coverage since 1/1/1997 (%)	94.6	83.4	47.7
	Coverage since first date with data (%)	95.1	93.2	58.1
	Coverage since first date of the shortest time series (%)	95.2	92.9	56.2
	Coverage since first date of the second shortest time series (%)	94.9	93.2	53.3
Precipitation	First date with data	5/17/97	1/1/99	1/1/00
	Last date with data	11/25/16	11/25/16	12/31/16
	Coverage since 1/1/1997 (%)	93.2	83.5	63.6
	Coverage since first date with data (%)	95.5	93.3	74.9
	Coverage since first date of the shortest time series (%)	95.9	95.1	74.9
	Coverage since first date of the second shortest time series (%)	95.5	93.3	70.5

Table S3 | Optimal parameter combinations for the mass balance model

Period	Bias (m)	Relative bias (%)	Temperature lapse rate (°C/km)	Precipitation lapse rate (mm/km)	DDF for snow (m $°C^{-1}d^{-1}$)	DDF for ice (m $°C^{-1}d^{-1}$)
Jul 2010 – Oct 2015	1.22	19.2	0	-6.2[3.0]**	0.008[0.004] **	0.004[0]**
Nov 2015* – May 2016	-0.05	3.5	-0.1	-6.7[3.1] **	0.008[0.004] **	0.001[0]**
May 2016 – Nov 2016	-0.12	2.9	0.1	-6.7[3.1] **	0.008[0.004] **	0.015[0]**

* Due to remaining gaps in the meteorological data, the period modeled was Jan – May 2016.
** Values in brackets correspond to ±1 standard deviation.
DDF stands for Degree Day Factors (see Supplementary Text)

Table S4 | SEACLID/CORDEX-SEA model output used in this study, including results from the statistical downscaling

Model Output Name	GCMs	Institution that developed the GCMs	RCMs	RCP	Downscaling results: Mean observation minus mean model		Downscaling results: Cramér-von Mises test [p-value]	
					T (°C)	Pp (mm/d)	T	Pp
MPI-M-MPI-ESM-MR	MPI-ESM-MR	Max Planck Institute for Meteorology, Germany	RegCM4	8.5	-0.14	2.72	3.94 [0.003]	19.22 [0]
				4.5	-0.15	0.6	4.49 [0.002]	2.78 [0.01]
IPSL-IPSL-CM5A-LR	IPSL-CM5A-LR	Institute Pierre-Simon Laplace, France	RegCM4	8.5	-0.21	-1.72	2.41 [0.015]	20.54 [0]
				4.5	0.09	-1.57	5.66 [0.001]	14.86 [0]
GFDL_REGCM4	GFDL-ESM2M	GFDL, USA	RegCM4	8.5	-0.15	0.72	4.35 [0.002]	0.92 [0.066]
				4.5	-0.13	0.85	2.54 [0.013]	1.29 [0.046]
CSIROMK36_REGCM4	CSIRO MK3.6	CSIRO, Australia	RegCM4	8.5	-0.08	0.5	2.41 [0.015]	0.88 [0.069]
				4.5	-0.08	0.53	2.97 [0]	0.78 [0.079]
CNRM5_REGCM4	CNRM-CM5	Centre National de Recherches Meteorologiques, France	RegCM4	8.5	-0.05	1.12	0.51 [0.1]	2.78 [0.01]
				4.5	-0.2	1.39	6.78 [0]	4.85 [0.001]

Table S5 | Descriptive statistics of δ^{18}O, δD and *d* (deuterium excess) in Cores D1 and D1B

	Min	Mean	Max	Range
Core D1				
δ^{18}O (‰)	-19.68	-16.07	-13.62	6.06
δD (‰)	-146.65	-116.36	-96.46	50.19
d (‰)	8.01	12.21	19.80	11.79
Core D1B				
δ^{18}O (‰)	-20.32	-16.41	-14.06	6.26
δD (‰)	-147.77	-116.87	-96.56	51.21
d (‰)	10.09	14.41	19.22	9.13

Table S6 | Reference matching points of δ^{18}O in Cores D1 and D1B with NINO3 ERSST (Fig. 5*B*). The 1964 bomb horizon (bold) was identified at 23.4 m depth in Core D1 and assuming the top layer represents the time when the ice cores were collected (May 2010).

Depth (meter)		Year
D1	D1B	
0.00	0.00	2010.4
3.97	4.25	2008
7.35	7.30	2003
8.25	8.15	2000
8.48	8.37	1998
9.80	9.40	1996
10.91	11.00	1992
12.02	12.06	1989
12.59	12.81	1987.5
14.92	14.23	1983
17.03	16.62	1975.5
19.54	19.34	1973
22.28	22.00	1966
23.39	**23.39**	**1964**

References

1. Klein AG, Kincaid JL (2006) Retreat of glaciers on Puncak Jaya, Irian Jaya, determined from 2000 and 2002 IKONOS satellite images. *J. Glaciol. 52*: 65-79.
2. Pfeffer WT, et al. (2014) The Randolph glacier inventory: A globally complete inventory of glaciers. *J. Glaciol*, 60: 537-552.
3. Bahr DB, Meier MF, Peckham SD (1997) The physical basis of glacier volume-area scaling. *J. Geophys. Res: Solid Earth*, 102: 20355-20362.
4. Gärtner-Roer I, Naegeli K, Huss M, Knecht T, Machguth H, Zemp M (2014) A database of worldwide glacier thickness observations. *Global Planet. Change*, 122: 330–344.
5. Fernández A, Mark BG (2016) Modeling modern glacier response to climate changes along the Andes Cordillera: A multiscale review. *J. Adv. Model. Earth. Sys.*, 8: 467-495.
6. NASA/METI/AIST/Japan Spacesystems, U.S./Japan ASTER Science Team (2009) ASTER Global Digital Elevation Model [Data set]. NASA EOSDIS Land Processes DAAC. doi: 10.5067/ASTER/ASTGTM.002
7. Hock R (2005) Glacier melt: A review of processes and their modelling. *Prog. Phys. Geogr: Earth and Environment*, 29: 362-391.
8. Juneng L, et al. (2016) Sensitivity of Southeast Asia rainfall simulations to cumulus and air-sea flux parameterizations in RegCM4. *Clim Res*, 69: 59-77.
9. Ngo-Duc T, et al. (2017) Performance evaluation of RegCM4 in simulating extreme rainfall and temperature indices over the CORDEX-Southeast Asia region. *Int. J. Climatol.*, 37: 1634-1647.
10. Cruz FT, et al. (2017) Sensitivity of temperature to physical parameterization schemes of RegCM4 over the CORDEX-Southeast Asia region. *Int. J. Climatol*., 37: 5139-5153.
11. Chung JX, Liew J, Fredolin T, Jamaluddin AF (2017) Performances of BATS and CLM land-surface schemes in RegCM4 in simulating precipitation over CORDEX Southeast Asia domain. *Int. J. Climatol*, 38: 794-810.
12. Taylor KE, Stouffer RJ, Meehl GA (2012) An overview of CMIP5 and the experiment design. *Bull. Am. Meteorol. Soc*, 93: 485-498.
13. Michelangeli PA, Vrac M, Loukos H (2009) Probabilistic downscaling approaches: Application to wind cumulative distribution functions. *Geophys. Res. Lett*., 36: 2–7.
14. Permana DS (2011) Climate, precipitation isotopic composition and tropical ice core analysis of Papua, Indonesia. Master thesis (Ohio State University, Ohio, USA).
15. Allison I (1976) In The Equatorial Glaciers of New Guinea (eds Hope, G. S., Peterson, J. A., Allison, I. & Radok, U.) 39-59 (A. A. Balkema, Rotterdam).
16. Schotterer U, Stichler W, Ginot P (2004) In Earth Paleoenvironments: Records preserved in mid- and low-latitude glaciers (eds Cecil, L. D., Green, J. R. & Thompson, L. G.) 39-59 (Kluwer Academic, Dordrecht).

17. Thompson LG, et al. (2002) Kilimanjaro ice core records: evidence of Holocene climate change in tropical Africa. *Science* 298: 589-593.
18. Van Der Wel LG, et al. (2011) Using high-resolution tritium profiles to quantify the effects of melt on two Spitsbergen ice cores. *J. Glaciol*, 57: 1087-1097.
19. Thompson LG, et al. (2013) Annually resolved ice core records of tropical climate variability over the past ~1800 years. *Science*. 304: 945-950.
20. Ebisuzaki, W. (1997). A method to estimate the statistical significance of a correlation when the data are serially correlated. *J. Clim*, *10*(9), 2147-2153.
21. Permana DS, Thompson LG, Setyadi G (2016) Tropical West Pacific moisture dynamics and climate controls on rainfall isotopic ratios in southern Papua, Indonesia. *J. Geophys. Res. Atmos*. 121: 2222-2245.
22. Moerman JW, et al. (2013). Diurnal to interannual rainfall $\delta^{18}O$ variations in northern Borneo driven by regional hydrology. *Earth Planet Sc Lett*. 369: 108-119.
23. Jarvis A, Guevara E, Reuter HI, Nelson AD (2008) Hole-filled SRTM for the globe: version 4: data grid. Available from the CGIAR-CSI SRTM 90m Database (http://srtm.csi.cgiar.org).
24. Alaska Satellite Facility Distributed Active Archive Center (ASF DAAC) (2015) ALOS-1 PALSAR_Radiometric_Terrain_Corrected_high_res. doi: 10.5067/Z97HFCNKR6VA.
25. Peterson TC, Vose RS (1997) An overview of the global historical climatology network temperature database. *Bull. Am. Meteorol. Soc. 78: 2837-2849.*
26. Compo GP, et al. (2011) The twentieth century reanalysis project. *Q. J. R. Meteorol. Soc.* 137: 1-28.